# Pathogenic Mutations Associated with Legius Syndrome Modify the Spred1 Surface and Are Involved in Direct Binding to the Ras Inactivator Neurofibromin

**Sebastian Führer**[1,2], **Martin Tollinger**[2] **and Theresia Dunzendorfer-Matt**[1]

***1 - Division of Biological Chemistry,*** *Biocenter, Medical University of Innsbruck, Innrain 80/82, 6020 Innsbruck, Austria*
***2 - Institute of Organic Chemistry and Center for Molecular Biosciences Innsbruck (CMBI),*** *University of Innsbruck, Innrain 80/82, 6020 Innsbruck, Austria*

***Correspondence to Theresia Dunzendorfer-Matt:*** *theresia.dunzendorfer-matt@i-med.ac.at*
https://doi.org/10.1016/j.jmb.2019.07.038
***Edited by Daniel L. Minor***

## Abstract

Neurofibromatosis type I (NF1) and Legius syndrome are rare inherited disorders that share diagnostic symptoms including dermal abnormalities like axillary and inguinal freckling and café au lait spots. In addition, patients suffering from NF1 have a demanding risk for the development of severe tumors of the peripheral and central nervous system among other NF1-specific symptoms. NF1 and Legius syndrome are caused by alterations in the NF1 and SPRED1 genes encoding the Ras inhibitors neurofibromin and Spred1 (sprouty related EVH1 domain-containing protein), respectively. Neurofibromin functions as a Ras-specific GTPase-activating protein (Ras-GAP), and Spred1 enhances Ras inactivation by recruiting neurofibromin from the cytosol to membrane-anchored Ras. In a previous study, we mapped the Spred binding site to the GAP-related domain of neurofibromin (NF1-GAP) and identified the GAPex subdomain as critical for Spred1 binding. Here, we characterize the binding site of these proteins in more detail focusing on a mutant Spred1 variant carrying a pathogenic missense mutation (threonine 102 to arginine). Introduction of this mutation, which locates at the N-terminal EVH1 domain of Spred1, weakens the interaction with neurofibromin by about 3 orders of magnitude without perturbing the protein fold, and the binding site of NF1-GAP on the mutant Spred1(EVH1) variant can be identified by NMR spectroscopy. Taken together, our data provide structural insight into the interaction of Spred1 and neurofibromin and characterize the structural or functional consequence of selected patient-derived mutations associated with Legius syndrome.


## Introduction

The Ras/mitogen-activated protein kinase (MAPK) pathway is frequently perturbed in human cancers due to sporadic or inherited mutations in the genes encoding the signaling protein components or their regulators. The protein Spred1 (sprouty related EVH1 domain containing protein 1) was identified as a specific inhibitor of the MAPK pathway [1] and acts as a tumor suppressor in early childhood malignancies and melanomas [2,3]. Legius syndrome is characterized by symptoms including pigmentary abnormalities like café au lait macules, and skin freckling and is caused by mutations in the human *SPRED1* gene [4–9]. This phenotype resembles the clinical picture of neurofibromatosis type I (NF1), an inherited syndrome where patients additionally present with more severe symptoms including bone deformations, benign neurofibromas and an elevated risk to develop malign tumors of the peripheral and central nervous system [10,11]. The human *NF1* gene, which is mutated in NF1 patients, encodes the giant (320 kDa) protein neurofibromin, which functions as a Ras-specific GTPase activating protein (GAP) that blocks Ras activity in cells. Beyond its role in neurofibromatosis, *NF1* mutations have also been linked to sporadic malignancies and neurofibromin has been described as the major RasGAP in several human tumors [12–17]. Stowe *et al.* [18] analyzed the role of Spred1 in the inhibition of the MAPK pathway and defined a shared molecular mechanism among the two symptomatically related diseases NF1 and Legius syndrome. They described a cytosolic complex containing Spred1 and

 

neurofibromin, which shuttles to the cell membrane and enhances inactivation of membrane bound Ras. Formation of this complex was dependent on the N-terminal Ena/VASP homology domain 1 (EVH1) of Spred1, which was demonstrated by using mutant variants of Spred1 derived from Legius syndrome patients. Specifically, pathogenic missense mutations on positions of Trp31 [19] and Thr102 [20] lead to weakening of the interaction below the detection limit of immunoprecipitation experiments. In a previous study, we defined the docking site of Spred1 on the giant neurofibromin protein and mapped it to the central 36-kDa Ras binding GAP related domain (also termed GRD) of neurofibromin [21]. The crystal structure of the neurofibromin(GAP) domain (NF1-GAP hereafter) consists of a module of two subdomains, namely, a 25-kDa central domain (GAPc), which is sufficient and required to bind and inactivate Ras, and an 11-kDa extra domain (GAPex), which is not in contact with Ras [22]. GAPex is formed by about either 50 residues that are located N-terminal and C-terminal to the GAPc region in the primary sequence and fold into six helices, and it is structurally conserved in other RasGAPs including synGAP, IQ-GAP, and p120GAP [23–25]. In our previous study, we could show that the neurofibromin GAPex domain is required for Spred1(EVH1) binding in cultivated cells, and we now aim at the detailed characterization of this interaction.

Some EVH1 domain containing proteins have been described as regulators of actin polymerization and are located at lamellipodia, at the leading edge of migrating cells. EVH1 domains exhibit a pleckstrin homology (PH)-like fold and are present in human proteins classified in four different families, namely, the Spred family (comprising Spred1, Spred2, and Spred3), which all bind neurofibromin [18]; the Homer family; the Ena family (homolog to drosophila enabled); and the Wiskott Aldrich syndrome protein family (WASP). Except for Spred, one member each of these families has been structurally characterized in its function of binding proline-rich sequences (PRSs). Peptide recognition involves three surface located aromatic and/or hydrophobic residues (Tyr/Ile, Trp, and Phe), which are conserved within these EVH1 domains [26–32]. The ligands harbor either an FPXφP motif, where φ denotes a hydrophobic and X any residue, or a PPXXF motif classifying the PRS as either belonging to class I or class II ligands [26]. Structural analysis of the *Xenopus tropicalis* Spred homolog revealed that the Spred1(EVH1) domain differs significantly from this hydrophobic surface pattern and a different binding mode involving less PRSs was suggested for the Spred family [33]. None of the above-mentioned classic EVH1 binding PRS motifs is present in the Spred1 binding NF1-GAPex subdomain and a region including two proline residues in NF1-GAPex (corresponding to Pro1527 and Pro1528) was shown to be dispensable for Spred binding [34]. Amino acid positions of non-truncating missense mutations described in Legius syndrome are evenly distributed over the EVH1 primary sequence and do not point to a specific binding site. Thus, the detailed binding mode of neurofibromin to its cellular recruitment protein Spred remains unclear.

Here we report the fine mapping of the binding site of the Ras-GAP neurofibromin to a specific site on the surface of the Spred1(EVH1) domain. Furthermore, we show the functional or structural consequence of selected mutations in Spred1 associated with Legius syndrome. Importantly, a threonine to arginine mutation diminishes NF1-GAP binding significantly, while the fold of the domain remains unchanged.

## Results and Discussion

In a previous study, we identified the GAP domain of neurofibromin as the primary binding site for the Spred1(EVH1) domain (see domain schemes in Fig. 1a and Ref. [21]). Non-truncating missense mutations associated with Legius syndrome (summarized in Table 1) are equally distributed over the primary sequence of the Spred1(EVH1) domain (Fig. 1b), and no mutational hotspot could be detected in this region. In our attempt to characterize the role of these mutations in neurofibromin binding, we assigned nuclear magnetic resonance signals of isotope-labeled Spred1(EVH1) [35] and performed titration experiments with unlabeled NF1-GAP. However, the high affinity [21] and the high molecular mass of the complex formed with wild-type Spred1(EVH1) preclude NMR chemical shift-based binding site mapping in Spred1(EVH1). While 99% of all non-proline backbone amide resonances in wild-type Spred1 (EVH1) can be observed in a $^{1}H^{15}N$ heteronuclear single quantum coherence (HSQC) experiment, only about 15% of these resonances are visible upon the addition of an equimolar amount of NF1-GAP (Fig. 1S). As a matter of fact, most of these residues are located at the C-terminus of the protein domain.

In order to characterize the function of pathogenic missense mutations in patients, we filtered the positions of mutations on the protein level for the following criteria: Since all three members of the Spred family (Spred1, Spred2, and Spred3) bind to neurofibromin, we selected the positions that are conserved within the Spred family (Fig. 1b). From this pool, we selected non-glycine residues whose side chains, according to the high resolution crystal structure of frog Spred1(EVH1) [33], point to the surface of the protein and are more likely responsible for protein recognition than for maintaining the fold of the EVH1 domain. A third filter selected residues that are located in a region of the EVH1 surface that has been shown to bind PRSs in other EVH1 domain

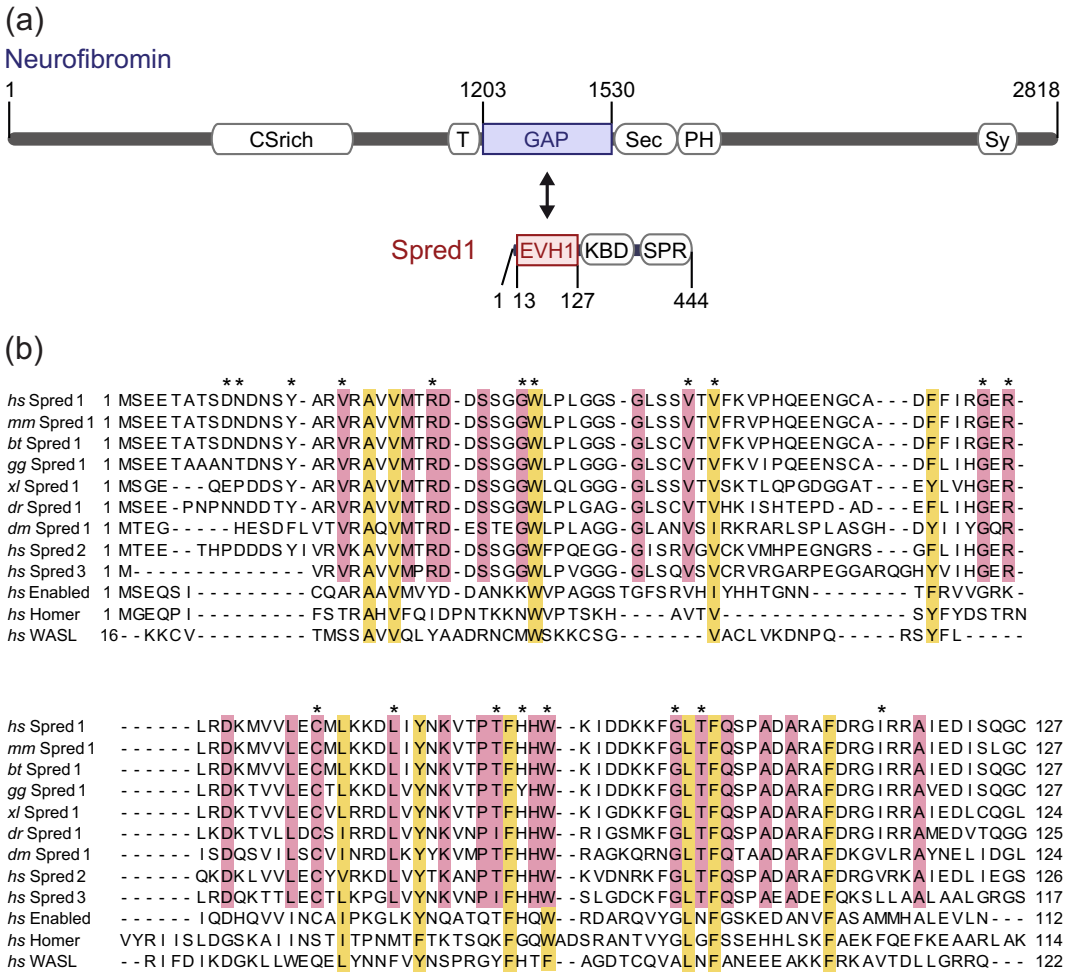


**Fig. 1.** Domain schemes of the human neurofibromin and Spred1 protein, and EVH1 sequence analysis. (a) Organization of neurofibromin and Spred1 showing domain boundaries for the interacting neurofibromin(GAP) and the Spred1(EVH1) constructs (blue and red rectangles) used in the present work. In addition, neurofibromin harbors a cysteine and serine-rich region (CSrich), a potential tubulin binding domain (T), a Sec14PH bipartite module (SecPH), and a potential syndecan binding domain (Sy). The c-Kit receptor binding region (KBD) and the C-terminal region known as Sprouty domain (SPR) of Spred1 are indicated. (b) Sequence alignment of the N-terminus of human Spred1 including the EVH1 domain with its mouse (*mm*), bovine (*bt*), chicken (*gg*), frog (*xl*), zebrafish (*dr*), and fruit fly (*dm*) homologs, and with members of the four EVH1 domain containing protein families: the Spred family (Spred2, Spred3), the Ena family (Enabled), the Homer family (Homer), and the Wiskott Aldrich syndrome protein family (WASL). Hydrophobic residues conserved in all EVH1 domains are highlighted in yellow, residues that are specifically conserved within the Spred family are highlighted in red, and positions of mutations found in Legius syndrome patients are indicated by asterisks. The alignment was generated using Chimera software and the MAFFT algorithm.

containing families. Those residues were identified by structural superposition of the respective PRS ligated EVH1 complexes [29,31,32] and using the superposition derived alignment together with Spred1(EVH1) sequences from other organisms and from human Spred2 and Spred3 (Fig. 1b). From these considerations, we conclude that a tryptophan residue at position 31 and a threonine residue at position 102 were the most likely candidates for residues that may be directly involved in neurofibromin binding. This was supported by an earlier finding that mutations at these positions reduced neurofibromin binding below the detection limit in cells and in pull-down experiments using diluted protein solutions [18,21]. We cloned and expressed Spred1(EVH1) harboring the pathogenic missense mutation Trp31Cys. In contrast to the well-soluble wild-type variant [21,35], introduction of this mutation apparently caused the formation of insoluble protein inclusion bodies during recombinant protein expression. The same was observed upon introduction of the Trp31Arg mutation (data not shown). However, replacement of threonine 102 by arginine (T102R) produced soluble protein that could

**Table 1.** Legius syndrome patient-derived non-truncating missense mutations in the EVH1 domain of Spred1, according to published data [4–6] and to the following databases: Leiden Open Variation Database (LOVD; http://www.lovd.nl/3.0/home), The Human Gene Mutation Database (HGMD; http://www.hgmd.cf.ac.uk), and Legius syndrome database (http://www.arup.utah.edu/database)

| Residue | Wild type | Patient mutation | Location/consequence |
|---|---|---|---|
| 1 | Met | Thr | N-Term, affects translation |
| 9 | Asp | Val, Glu | No structural data available |
| 10 | Asn | Lys | No structural data available |
| 14 | Tyr | Tyr | β-Sheet, surface, modulates NF1-binding |
| 17 | Val | Ile | β-Sheet, surface |
| 24 | Arg | Gln | Loop, surface, modulates NF1-binding |
| 30 | Gly | Arg | Loop, surface, modulates NF1-binding |
| 31 | Trp | Arg, Leu, Cys | β-Sheet, surface, impairs protein folding |
| 42 | Val | Ile | β-Sheet, core |
| 44 | Val | Asp | β-Sheet, core |
| 62 | Gly | Arg | β-Sheet, core |
| 64 | Arg | Gln | Loop, surface |
| 74 | Cys | Phe | β-Sheet, surface |
| 80 | Leu | Arg | Loop, core |
| 88 | Thr | Lys | Loop, surface, modulates NF1-binding |
| 90 | His | Gln | β-Sheet, surface, modulates NF1-binding |
| 92 | Trp | Arg | β-Sheet, core |
| 100 | Gly | Asp | β-Sheet, core |
| 102 | Thr | Lys, Arg, Met | β-Sheet, surface, (Arg) reduces affinity for NF1-GAP |
| 116 | Ile | Asn | α-Helix, core |

be characterized in detail by solution NMR spectroscopy, and a complete backbone resonance assignment of this mutant was obtained (Fig. 2a). Based on the NMR chemical shift data, we determined a CS-Rosetta structural model [36] of Spred1 (EVH1)*T102R, which shows that the canonical EVH1 fold is preserved in this mutant and the global structure of the domain remains unchanged when compared to the wild type protein (Fig. 2b).

We used this mutant variant and analyzed its ability to form complexes with NF1-GAP at different concentrations. Analytical size exclusion chromatography combined with light scattering and refractive index detection was performed in order to compare the formation of NF1-GAP complexes with wild type and mutant Spred1(EVH1). We observed masses of 13,658 [assigned to Spred1(EVH1), $M_{calc}$ = 13,494], 14,045 [assigned to $^{15}$N-Spred1(EVH1)*T102R, $M_{calc}$ = 13,720], and 40,777 [NF1-GAP, $M_{calc}$ = 40,127] in the light scattering and UV profiles derived for the individual injections of the proteins. Analysis of protein mixtures revealed an additional peak for which a mass of 52,174 was detected [NF1-GAP + Spred1(EVH1), $M_{calc}$ = 53,621], which suggests the formation of an NF1-GAP/Spred1 (EVH1) complex. We have previously shown that the EVH1 domain forms a stable complex with NF1-GAP, which can be isolated from an analytical size exclusion column [21]. However, introduction of the T102R mutation weakened the affinity significantly, and no peak shift indicating complex formation could be detected (Fig. 3a). Surface plasmon resonance (SPR) experiments revealed a $K_d$ of 6.6 μM for Spred1(EVH1)*T102R binding to NF1-GAP (Figs. 3b and S2), which is 3 orders of magnitude higher than the previously determined $K_d$ of 7.4 nM for the wild-type protein [21].

The lower affinity of the NF1-GAP/Spred1(EVH1) *T102R complex is in the range at which binding site mapping by NMR is possible. In a titration experiment, unlabeled NF1-GAP was added to the $^{15}$N-labeled mutant EVH1 domain in order to identify residues that change their chemical shifts upon complex formation (Fig. 4a and b). All backbone amide resonances in Spred1(EVH1)*T102R can still be identified in $^{1}$H$^{15}$N HSQC experiments after the addition of an equimolar amount of NF1-GAP. Two stretches with chemical shift changes ($\Delta\delta_{obs} > 0.01$ ppm) upon complex formation are present in the EVH1 domain, that is, the region between Thr23 and Gly35 (including residues Arg24, Asp25, and Gly29, which display the largest $\Delta\delta_{obs}$ values) and the region between Asn83 and Lys93 (Fig. 4b). These positions form a contiguous patch on the Spred1(EVH1) protein surface indicating the NF1-GAP binding site, as visualized on the crystal structure of *X. tropicalis* Spred1(EVH1) (Fig. 5a). Arg24, Asn83, His90, and His91 show shifts upon ligand binding. Corresponding positions in other EVH1 family members, defined by structural superposition, are in close proximity to the proline-rich ligand in the respective complex structures, supporting the hypothesis that neurofibromin uses a similar binding site. Our *in vitro* data are in good agreement with a previous study in yeast, where missense mutations causing exchange of Gly30, Trp31, Thr88, and Trp92 in the EVH1 domain made a significant impact on the interaction with an NF1-GAP isoform carrying a 21-amino-acid insertion in the GAPcore domain. [34]. As a side note, this isoform arising from alternative splicing of exon 23 [37] is also capable of binding to Spred1, although quantitative data are not available.

Our finding raised the question whether the footprint of neurofibromin on the surface of Spred1 could be linked to Legius syndrome. Indeed, 10 out of 14 currently known patient-derived missense mutation positions in the EVH1 domain of Spred1 show a chemical shift perturbation upon addition of NF1-GAP. The position of patient-derived non-truncating missense mutations is displayed on the surface of the EVH1 domain (Fig. 5b). Interestingly, this cluster of patient mutation positions overlaps significantly with the residues that are involved in neurofibromin binding (compare Fig. 5a and b).

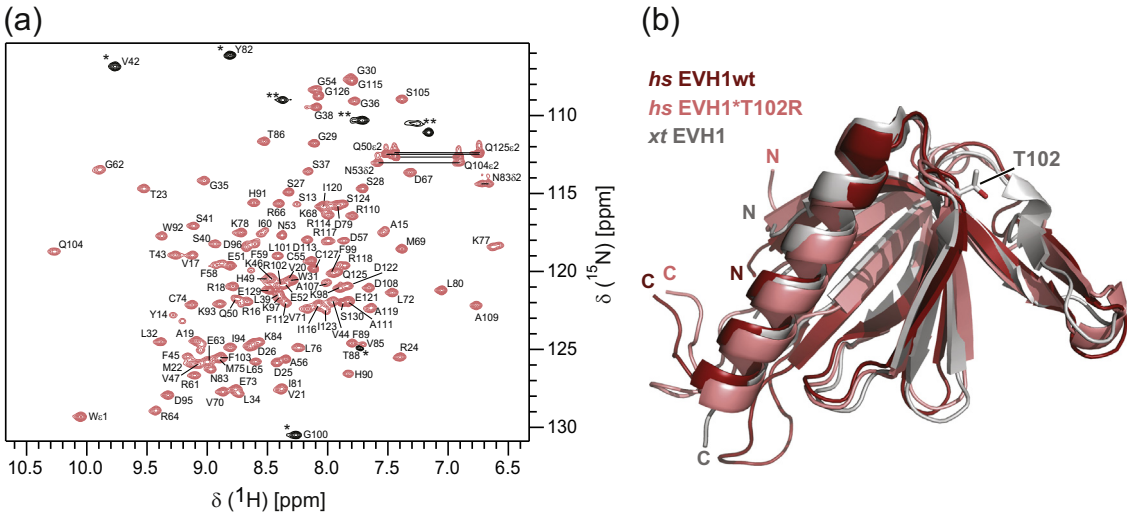


**Fig. 2.** Structural model of Spred1(EVH1) carrying the pathogenic T102R mutation. (a) $^{1}H^{15}N$ HSQC spectrum of $^{15}N$-labeled Spred1(EVH1)*T102R recorded on a 500 MHz spectrometer at 298 K. Resonance assignments are shown, with the numbering corresponding to the human Spred1 protein, except for the position of the mutation. Horizontal lines indicate asparagine and glutamine $NH_2$ side-chain resonances, aliased signals (black) are labeled by asterisks, and signals that likely arise from arginine side chains (ε-NH) are labeled by two asterisks. Resonance assignments are available online at the BMRB repository (accession number 27793). (b) Overlay of the chemical shift-based Rosetta models of human wild-type (red) and mutant (light red) Spred1(EVH1) with the crystal structure of the frog Spred1 homolog (PDB 1XOD, gray) demonstrated identical folds.

NMR relaxation experiments on the homologous EVH1 domain of the *Schizosaccharomyces pombe* Dcp1 protein revealed significant conformational flexibility of the aromatic binding groove in the free state [38]. We were interested whether conformational flexibility is a common feature of binding grooves in the Spred1(EVH1) domain and performed NMR relaxation experiments. To experimentally characterize picosecond-to-nanosecond time scale flexibility of wild-type Spred1(EVH1) and Spred1(EVH1)*T102R, we determined the backbone amide order parameters, $S^2$. The experimental data reveal a highly flexible region between residues Met22 and Leu32 in the wild-type protein and in the T102R variant with order parameters below 0.7 (Fig. S3). Evidently, this region coincides with the NF1-GAP binding site that was derived from NMR chemical shift data. Structural flexibility may be a benchmark for regions that play a role in protein interactions. It is thus tempting to speculate that inherent flexibility of Spred1(EVH1) at the NF1-GAP binding site might contribute to interaction between these two proteins. Another flexible region in Spred1 (EVH1) includes residues His49 to Phe58. This region comprises a long and surface-exposed loop between β-strands 2′ and 3 that is distal from the NF1-GAP binding site and may not be involved in binding.

Taken together, we showed that the patient-derived mutant Spred1(EVH1)*T102R, which has a markedly lower affinity to the neurofibromin GAP domain than wild-type Spred1(EVH1), displays the canonical EVH1 fold. Due to the relatively low affinity between Spred1(EVH1)*T102R and NF1-GAP, the binding surface on the Spred1(EVH1) domain could be mapped by nuclear magnetic resonance experiments, revealing an expanded yet contiguous patch on the protein surface that overlaps with a significant number of patient mutations known to date. This suggests that loss of neurofibromin-Spred1 binding due to mutations in Spred1 is one of the major reasons for the development of Legius syndrome. Since the other Spred family member Spred2 also binds neurofibromin [18] and may partially compensate for loss of Spred1 in neurofibromin-dependent Ras inactivation, the phenotype of Legius syndrome is comparatively mild. Alterations in neurofibromin, however, are in general associated with a severe phenotype. Its function as a major negative regulator of Ras can obviously not be compensated by other RasGAPs.

## Materials and Methods

### *In silico* analysis

The alignment was generated by superposition of EVH1 structures (PDB codes in brackets) solved for one member each of the four families, namely, Spred1 (3SYX), Ena (1EVH), Homer (1DDW), and N-Wasp (1MKE) using Chimera software. Corresponding positions in the 3D structure were aligned in a linear sequence and set as input for an

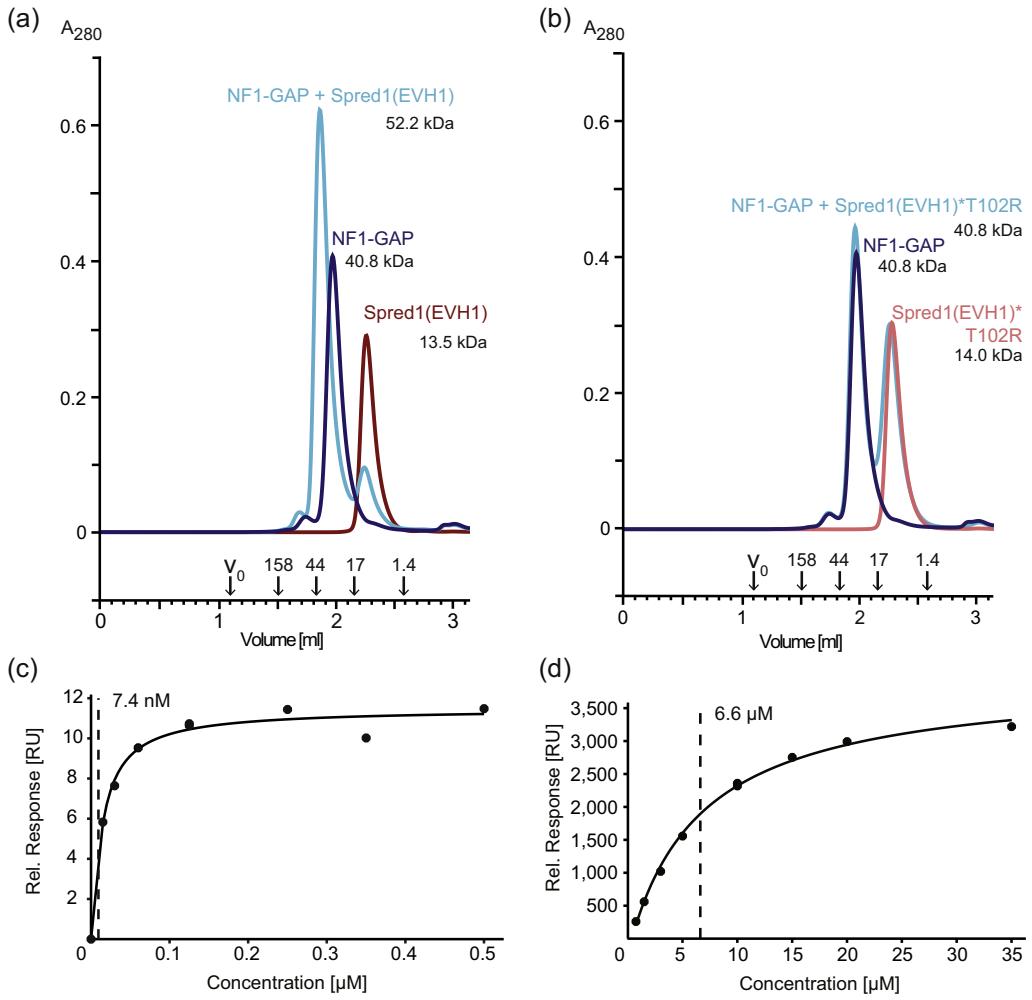


**Fig. 3.** Comparison of NF1-GAP binding to wild type and mutant Spred1(EVH1). Size exclusion chromatography experiments using purified NF1-GAP together with (a) either Spred1(EVH1) in wild-type form or (b) a variant carrying the pathogenic mutation T102R. Proteins were injected individually (chromatograms for NF1-GAP are shown in blue; Spred1 (EVH1) and Spred1(EVH1)*T102R are shown in red and light-red, respectively), or in 1:1 stoichiometric mixtures (chromatograms in cyan) to an analytical size exclusion column. Molecular masses calculated from online refractive index (RI) and multiple-angle light scattering (MALS) detection at the peak maxima are displayed. The void volume ($V_0$) of the gel filtration column and the elution volume of size standards (in kDa) are indicated by arrows. (c) Spred1(EVH1) or (d) Spred1 (EVH1)*T102R was titrated over immobilized His-tagged NF1-GAP in an SPR spectroscopy experiment and revealed affinities of 7.4 nM or 6.6 μM, respectively.

alignment calculation using the MAFF-T algorithm together with the following sequence entries (listed from top to bottom as they appear in Fig. 1b): NP_689807.1, NP_277059.1, NP_001179445.1, NP_001186638.1, NP_001121277.1, NP_998397.1, NP_610988.1, AAP59415.1, AAI51137.1, NP_001008493.1, AAH47438.1, and EAL24333.1.

### Plasmid construct generation

The construction of a plasmid encoding Asp1203–His1530, which represents the GTPase activating protein domain (NF1-GAP) of human neurofibromin isoform 2 (accession no. NP_000258.1) modified with a tabacco etch virus protease-cleavable N-terminal $(His)_6$-tag, has been described [21]. A cDNA encoding the EVH1 domain (Ser13–Ser130) of human Spred1 (accession no. NP_689807.1) in its wild-type form and in two variants encoding either one of the mutations Thr102Arg and Trp31Cys was generated by gene synthesis and inserted into pET21d as described [21].

Mutations, in order to generate the expression construct encoding Spred1(EVH1)*W31R, were introduced by site-directed mutagenesis using Phusion DNA polymerase (New England Biolabs)

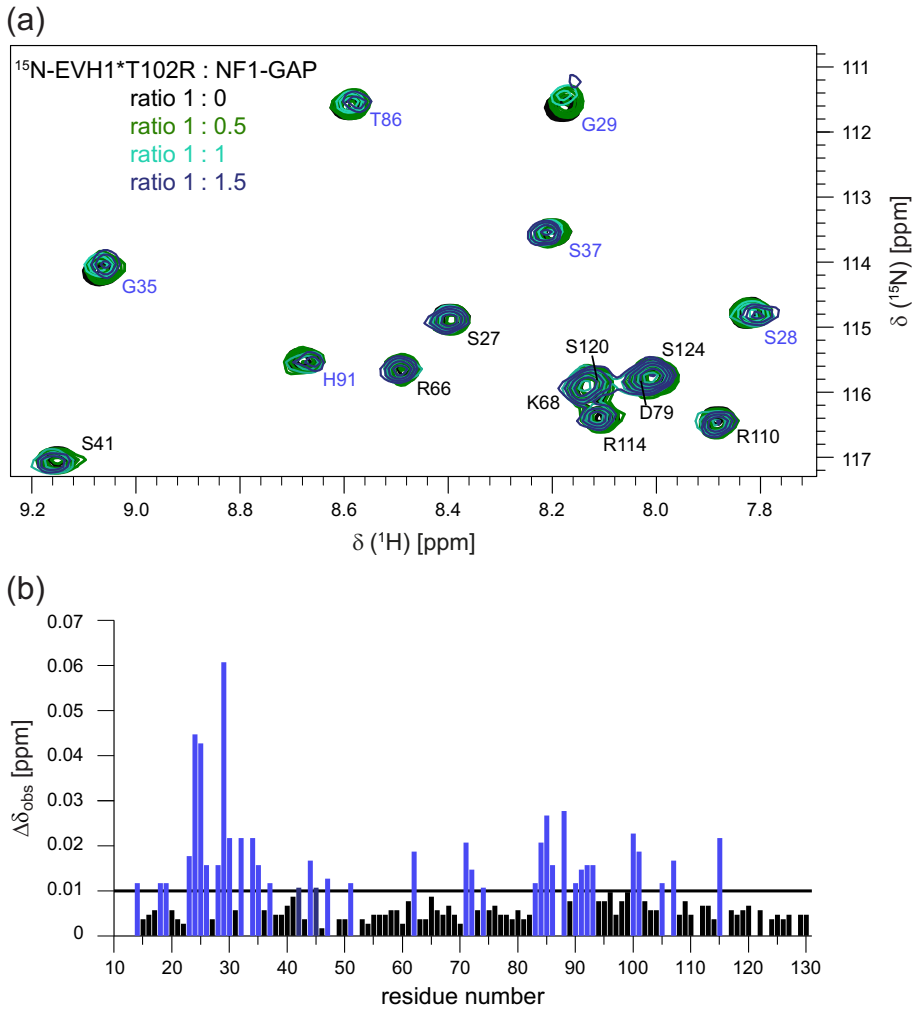


**Fig. 4.** Identification of residues on the Spred1(EVH1) surface that are involved in NF1-GAP binding. (a) Overlay of a section from the $^{1}H^{15}N$ HSQC spectra of $^{15}N$-labeled Spred1(EVH1)*T102RR recorded before (black) and after addition of unlabeled NF1-GAP in 0.5-fold (green), 1-fold (cyan), and 1.5-fold molar ratio (blue). Signals that show a chemical shift perturbation ($\Delta\delta_{obs}$) > 0.01 ppm are labeled in blue. (b) Chemical shift perturbations in $^{1}H^{15}N$ HSQC spectra of $^{15}N$-labeled Spred1(EVH1)*T102R upon addition of unlabeled NF1-GAP (1:1.5 ratio), bars with $\Delta\delta_{obs}$ > 0.01 ppm, are labeled in blue.

together with the oligonucleotides: 5′-gatagcagcggtggtcggctgccgctgggtg-3′ and 5′-cacccagcggcagccgaccaccgctgctatc-3′ (mutated nucleotides are underlined) according to the manufacturer's protocol. Successful introduction of the mutation was verified by DNA-sequencing.

### Protein expression and purification

The expression and purification of NF1-GAP and of Spred1(EVH1) have been described [21,35]. Spred1(EVH1)*T102R was essentially prepared as described for the wild-type protein, with the exception that the pH in the size exclusion chromatography buffer was set to 6.0.

### Analytical size exclusion chromatography with RI-MALS detection

Protein concentration of the samples was determined *via* differential refractive index detection at constant temperature, which is more exact than UV absorption-based quantification. Analytical size exclusion chromatography was performed on a gel filtration column (Superdex 200 Increase (5/150), GE Healthcare) which was connected to an HPLC system (Dionex, Thermo Scientific) and equilibrated in a buffer containing 20 mM Tris (pH 8.0), 150 mM NaCl, and 2 mM $MgCl_2$. Proteins were injected individually at 100 µM concentration or in 1:1 stoichiometric mixtures. The eluate from the column

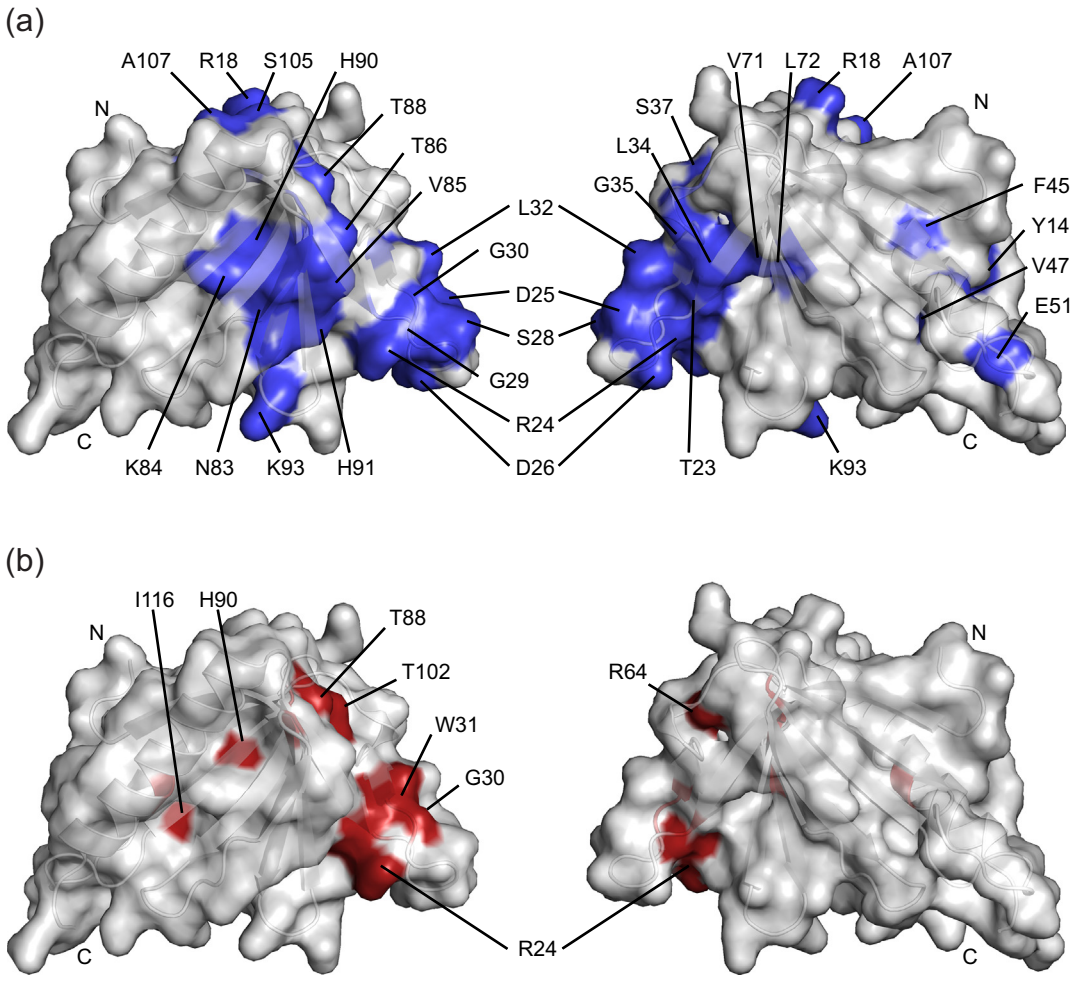


**Fig. 5.** Linkage analysis of residue positions modulated by NF1-GAP addition and selected patient-derived mutations. (a) Corresponding residue positions with surface-located side chains that show a perturbed chemical shift in the titration experiments shown in Fig. 4 and (b) positions of surface located patient-derived missense mutations are displayed (red) on the crystal structure of the *X. tropicalis* Spred1(EVH1) domain (PDB 1XOD). The N- and C-termini are indicated.

was analyzed for UV absorbance at 280 nm followed by online detection of multiple-angle light scattering (miniDAWN TREOS, WYATT) and of the refractive index at 298.20 K (Optilab T-rEX, WYATT). Data were analyzed using ASTRA 7 software.

### SPR experiments

SPR experiments were performed on a Biacore X100 system (GE Healthcare) essentially as described [21]. Dilution series of 15 to 500 nM Spred1 (EVH1) and 0.75 to 35 μM Spred1(EVH1)*T102R were prepared and injected over immobilized NF1-GAP. One sample of each dilution series was measured in duplicates [125 nM of Spred1(EVH1) and 10 μM of Spred1(EVH1)*T102R] to ensure reproducibility. Data collection was performed with a contact time of 60 s/540 s, a dissociation time of 120 s/240 s and a flow rate of (30 μL/min)/(10 μL/min) for Spred1(EVH1) or Spred1(EVH1)*T102R, respectively. At least two independent titration experiments were performed, and results were averaged. The dissociation constant $K_d$ was determined by nonlinear fitting of the sensorgrams to a 1:1 interaction model.

### NMR spectroscopy

All NMR experiments were performed at 298 K on a 500 MHz Agilent DirectDrive 2 spectrometer equipped with a room-temperature HCN triple-resonance probe. Data were processed with NMRPipe [39] and analyzed with CcpNmr [40] software. Backbone resonance assignments of Spred1(EVH1)*T102R were achieved by $^{1}H^{15}N$ HSQC and three-dimensional HNCACB, HN(CO)CACB, and HNCO experiments using $^{13}C$- and/or $^{15}N$-labeled Spred1(EVH1)*T102R at 0.6 or 1.2 mM, respectively, supplemented with 10% $D_2O$ (v/v). With the exception of the N-terminal methionine residue and the following non-native glycine, we were able to assign

all backbone amide resonances of Spred1(EVH1) *T102R. In addition, Cα and Cβ resonance assignments are 100% complete, while 95% of backbone C′ resonances could be assigned.

Measurements of backbone relaxation data [longitudinal and rotating-frame relaxation rates ($R_1$ and $R_{1\rho}$) and $^{15}N\{^1H\}$ steady-state NOE (nuclear Overhauser effect)] [41–44] were carried out with a spectral width of 1300 Hz in the $^{15}N$ dimension and of 8012 Hz in the $^1H$ dimension. Longitudinal relaxation periods were 11.1, 55.5, 111, 222, 333, 444, 555, and 666 ms with repeat experiments of 55.5 and 333 ms, and rotating-frame relaxation periods were 10, 20, 30, 40, 50, 70, and 90 ms with repeat experiments of 20 and 50 ms. The transverse relaxation rate ($R_2$) was calculated based on $R_1$ and $R_{1\rho}$ [45]. For $^{15}N\{^1H\}$ steady-state NOE measurements, HSQC spectra with (d1 = 3 s, sat = 1.25 s) and without saturation (d1 = 4.25 s) of the amide protons were recorded. Relaxation rates were determined using an in-house MATLAB fitting program. Order parameters $S^2$ were determined for all 95 of 118 amino acid resonances that are resolved in two-dimensional $^1H^{15}N$ spectra using the model-free approach [46–48] implemented in the Modelfree software (version 4.15) [49]. Mean order parameters were calculated for Tyr14–Asp122 using a sliding window of three amino acid residues.

NMR titration experiments were performed by recording $^1H^{15}N$ HSQC spectra of $^{15}N$-Spred1 (EVH1)*T102R (100 μM) in 20 mM sodium phosphate (pH 6.0), 200 mM NaCl, and 2 mM DTT supplemented with 10% (v/v) $D_2O$ before and after the addition of NF1-GAP in the same buffer. Molar ratios were 1: 4, 1: 3, 1: 1.5, 1: 1, 1: 0.5, and 1: 0.25 for $^{15}N$-Spred1(EVH1) *T102R: NF1-GAP. We used the combined amide chemical shift perturbation (CSP) $\Delta\delta_{obs}$ to identify amino acid residues that are involved in binding to NF1-GAP. The CSP values were calculated as follow: $\Delta\delta_{obs} = [((\Delta\delta_H)^2 + (\Delta\delta_N/5)^2)/2]^{1/2}$ [50]. We used a threshold value of 0.01 to define which amino acid residues are affected by binding of NF1-GAP.

### Accession numbers

NMR chemical shift assignment data have been deposited in the Biological Magnetic Resonance Data Bank (BMRB Entry ID 27793).

Supplementary data to this article can be found online at https://doi.org/10.1016/j.jmb.2019.07.038.

## Acknowledgments

We are grateful to Angela Ausserbichler and Linda Ahammer for excellent technical assistance, Johanna Gostner for support at the SPR system, and Klaus Scheffzek for providing reagents and lab space. T.D.M. gratefully acknowledges financing by the Austrian Cancer Society Tirol (14016). S.F. was supported by a PhD stipend of the University of Innsbruck, Austria. This work was supported by the Austrian Research Promotion Agency FFG (West Austrian BioNMR 858017).

*Received 3 June 2019;*
*Received in revised form 29 July 2019;*
*Accepted 31 July 2019*
Available online 8 August 2019

***Keywords:***
protein interaction;
NMR resonance assignment;
surface plasmon resonance;
Ras/MAPK pathway;
recombinant protein

***Abbreviations used:***
EVH1, Ena/VASP homology domain 1; HSQC, heteronuclear single quantum coherence; NF1, neurofibromatosis type I; NOE, nuclear Overhauser effect; SPR, surface plasmon resonance; Spred1, sprouty-related EVH1 domain containing protein 1.

## References

[1] T. Wakioka, A. Sasaki, R. Kato, T. Shouda, A. Matsumoto, K. Miyoshi, et al., Spred is a sprouty-related suppressor of Ras signalling, Nature. 412 (2001) 647–651.
[2] E. Pasmant, B. Gilbert-Dussardier, A. Petit, B. de Laval, A. Luscan, A. Gruber, et al., SPRED1, a RAS MAPK pathway inhibitor that causes Legius syndrome, is a tumour suppressor downregulated in paediatric acute myeloblastic leukaemia, Oncogene. 34 (2015) 631–638.
[3] J. Ablain, M. Xu, H. Rothschild, R.C. Jordan, J.K. Mito, B.H. Daniels, et al., Human tumor genomics and zebrafish modeling identify SPRED1 loss as a driver of mucosal melanoma, Science. (2018) 1055–1060.
[4] H. Brems, M. Chmara, M. Sahbatou, E. Denayer, K. Taniguchi, R. Kato, et al., Germline loss-of-function mutations in SPRED1 cause a neurofibromatosis 1-like phenotype, Nat. Genet. 39 (2007) 1120–1126.
[5] H. Brems, E. Legius, Legius syndrome, an update. Molecular pathology of mutations in SPRED1, Keio J Med. 62 (2013) 107–112.
[6] H. Brems, E. Pasmant, R. Van Minkelen, K. Wimmer, M. Upadhyaya, E. Legius, et al., Review and update of SPRED1 mutations causing Legius syndrome, Hum. Mutat. 33 (2012) 1538–1546.
[7] T.M. Muram-Zborovski, D.A. Stevenson, D.H. Viskochil, D.C. Dries, A.R. Wilson, M. Rong, SPRED 1 mutations in a neurofibromatosis clinic, J. Child Neurol. 25 (2010) 1203–1209.
[8] E. Spencer, J. Davis, F. Mikhail, C. Fu, R. Vijzelaar, E.H. Zackai, et al., Identification of SPRED1 deletions using

RT-PCR, multiplex ligation-dependent probe amplification and quantitative PCR, Am. J. Med. Genet. A 155A (2011) 1352–1359.
[9] G. Spurlock, E. Bennett, N. Chuzhanova, N. Thomas, H.P. Jim, L. Side, et al., SPRED1 mutations (Legius syndrome): another clinically useful genotype for dissecting the neurofibromatosis type 1 phenotype, J. Med. Genet. 46 (2009) 431–437.
[10] M.C.D.N. Upadhyaya, Neurofibromatosis Type 1: Molecular and Cellular Biology, Springer, 2012.
[11] Riccardi V.M. Neurofibromatosis, Phenotype Natural History, and Pathogenesis, Second edition The Johns Hopkins University Press, Baltimore and London, 1992.
[12] P.S. Dischinger, E.A. Tovar, C.J. Essenburg, Z.B. Madaj, E.E. Gardner, M.E. Callaghan, et al., NF1 deficiency correlates with estrogen receptor signaling and diminished survival in breast cancer, NPJ Breast Cancer. 4 (2018) 29.
[13] C. Philpott, H. Tovell, I.M. Frayling, D.N. Cooper, M. Upadhyaya, The NF1 somatic mutational landscape in sporadic human cancers, Hum Genomics. 11 (2017) 13.
[14] N. Sangha, R. Wu, R. Kuick, S. Powers, D. Mu, D. Fiander, et al., Neurofibromin 1 (NF1) defects are common in human ovarian serous carcinomas and co-occur with TP53 mutations, Neoplasia. 10 (2008) 1362–1372 (following 72).
[15] R.G. Verhaak, K.A. Hoadley, E. Purdom, V. Wang, Y. Qi, M.D. Wilkerson, et al., Integrated genomic analysis identifies clinically relevant subtypes of glioblastoma characterized by abnormalities in PDGFRA, IDH1, EGFR, and NF1, Cancer Cell 17 (2010) 98–110.
[16] L. Ding, G. Getz, D.A. Wheeler, E.R. Mardis, M.D. McLellan, K. Cibulskis, et al., Somatic mutations affect key pathways in lung adenocarcinoma, Nature. 455 (2008) 1069–1075.
[17] D.W. Parsons, S. Jones, X. Zhang, J.C. Lin, R.J. Leary, P. Angenendt, et al., An integrated genomic analysis of human glioblastoma multiforme, Science. 321 (2008) 1807–1812.
[18] I.B. Stowe, E.L. Mercado, T.R. Stowe, E.L. Bell, J.A. Oses-Prieto, H. Hernandez, et al., A shared molecular mechanism underlies the human rasopathies Legius syndrome and neurofibromatosis-1, Genes Dev. 26 (2012) 1421–1426.
[19] E. Denayer, M. Chmara, H. Brems, A.M. Kievit, Y. van Bever, A.M. Van den Ouweland, et al., Legius syndrome in fourteen families, Hum. Mutat. 32 (2011) E1985–E1998.
[20] L. Messiaen, S. Yao, H. Brems, T. Callens, A. Sathienkijkanchai, E. Denayer, et al., Clinical and mutational spectrum of neurofibromatosis type 1-like syndrome, JAMA. 302 (2009) 2111–2118.
[21] T. Dunzendorfer-Matt, E.L. Mercado, K. Maly, F. McCormick, K. Scheffzek, The neurofibromin recruitment factor Spred1 binds to the GAP related domain without affecting Ras inactivation, Proc. Natl. Acad. Sci. U. S. A. 113 (2016) 7497–7502.
[22] K. Scheffzek, M.R. Ahmadian, L. Wiesmuller, W. Kabsch, P. Stege, F. Schmitz, et al., Structural analysis of the GAP-related domain from neurofibromin and its implications, EMBO J. 17 (1998) 4313–4327.
[23] V.B. Kurella, J.M. Richard, C.L. Parke, L.F. Lecour Jr., H.D. Bellamy, D.K. Worthylake, Crystal structure of the GTPase-activating protein-related domain from IQGAP1, J. Biol. Chem. 284 (2009) 14857–14865.
[24] V. Pena, M. Hothorn, A. Eberth, N. Kaschau, A. Parret, L. Gremer, et al., The C2 domain of SynGAP is essential for stimulation of the Rap GTPase reaction, EMBO Rep. 9 (2008) 350–355.
[25] K. Scheffzek, A. Lautwein, W. Kabsch, M.R. Ahmadian, A. Wittinghofer, Crystal structure of the GTPase-activating domain of human p120GAP and implications for the interaction with Ras, Nature. 384 (1996) 591–596.
[26] L.J. Ball, T. Jarchau, H. Oschkinat, U. Walter, EVH1 domains: structure, function and interactions, FEBS Lett. 513 (2001) 45–52.
[27] M. Barzik, U.D. Carl, W.D. Schubert, R. Frank, J. Wehland, D.W. Heinz, The N-terminal domain of Homer/Vesl is a new class II EVH1 domain, J. Mol. Biol. 309 (2001) 155–169.
[28] K. Niebuhr, F. Ebel, R. Frank, M. Reinhard, E. Domann, U.D. Carl, et al., A novel proline-rich motif present in ActA of *Listeria monocytogene*s and cytoskeletal proteins is the ligand for the EVH1 domain, a protein module present in the Ena/VASP family, EMBO J. 16 (1997) 5433–5444.
[29] K.E. Prehoda, D.J. Lee, W.A. Lim, Structure of the enabled/VASP homology 1 domain-peptide complex: a key component in the spatial control of actin assembly, Cell. 97 (1999) 471–480.
[30] P.J. Renfranz, M.C. Beckerle, Doing (F/L)PPPPs: EVH1 domains and their proline-rich partners in cell polarity and migration, Curr. Opin. Cell Biol. 14 (2002) 88–103.
[31] B.F. Volkman, K.E. Prehoda, J.A. Scott, F.C. Peterson, W.A. Lim, Structure of the N-WASP EVH1 domain–WIP complex: insight into the molecular basis of Wiskott–Aldrich syndrome, Cell. 111 (2002) 565–576.
[32] J. Beneken, J.C. Tu, B. Xiao, M. Nuriya, J.P. Yuan, P.F. Worley, et al., Structure of the Homer EVH1 domain-peptide complex reveals a new twist in polyproline recognition, Neuron. 26 (2000) 143–154.
[33] N.J. Harmer, J.M. Sivak, E. Amaya, T.L. Blundell, 1.15 Angström crystal structure of the *X. tropicalis* Spred1 EVH1 domain suggests a fourth distinct peptide-binding mechanism within the EVH1 family, FEBS Lett. 579 (2005) 1161–1166.
[34] Y. Hirata, H. Brems, M. Suzuki, M. Kanamori, M. Okada, R. Morita, et al., Interaction between a domain of the negative regulator of the Ras-ERK pathway, SPRED1 protein, and the GTPase-activating protein-related domain of neurofibromin is implicated in Legius syndrome and neurofibromatosis type 1, J. Biol. Chem. 291 (2016) 3124–3134.
[35] S. Führer, L. Ahammer, A. Ausserbichler, K. Scheffzek, T. Dunzendorfer-Matt, M. Tollinger, NMR resonance assignments of the EVH1 domain of neurofibromin's recruitment factor Spred1, Biomol NMR Assign. 11 (2017) 305–308.
[36] Y. Shen, O. Lange, F. Delaglio, P. Rossi, J.M. Aramini, G. Liu, et al., Consistent blind protein structure generation from NMR chemical shift data, Proc. Natl. Acad. Sci. U. S. A. 105 (2008) 4685–4690.
[37] L.B. Andersen, R. Ballester, D.A. Marchuk, E. Chang, D.H. Gutmann, A.M. Saulino, et al., A conserved alternative splice in the von Recklinghausen neurofibromatosis (NF1) gene produces two neurofibromin isoforms, both of which have GTPase-activating protein activity, Mol. Cell. Biol. 13 (1993) 487–495.
[38] J.P. Wurm, J. Overbeck, R. Sprangers, The *S. pombe* mRNA decapping complex recruits cofactors and an Edc1-like activator through a single dynamic surface, RNA. 22 (2016) 1360–1372.
[39] F. Delaglio, S. Grzesiek, G.W. Vuister, G. Zhu, J. Pfeifer, A. Bax, NMRPipe: a multidimensional spectral processing system based on UNIX pipes, J. Biomol. NMR 6 (1995) 277–293.
[40] W.F. Vranken, W. Boucher, T.J. Stevens, R.H. Fogh, A. Pajon, M. Llinas, et al., The CCPN data model for NMR spectroscopy: development of a software pipeline, Proteins. 59 (2005) 687–696.

[41] G. Barbato, M. Ikura, L.E. Kay, R.W. Pastor, A. Bax, Backbone dynamics of calmodulin studied by 15N relaxation using inverse detected two-dimensional NMR spectroscopy: the central helix is flexible, Biochemistry. 31 (1992) 5269–5278.
[42] L.E. Kay, L.K. Nicholson, F. Delaglio, A. Bax, D.A. Torchia, Pulse sequences for removal of the effects of cross correlation between dipolar and chemical-shift anisotropy relaxation mechanisms on the measurement of heteronuclear T1 and T2 values in proteins, J. Magn. Reson. 97 (1991) 359–375.
[43] D.M. Korzhnev, V.Y. Orekhov, L.E. Kay, Off-resonance R (1rho) NMR studies of exchange dynamics in proteins with low spin-lock fields: an application to a Fyn SH3 domain, J. Am. Chem. Soc. 127 (2005) 713–721.
[44] D.M. Korzhnev, V.Y. Orekhov, F.W. Dahlquist, L.E. Kay, Off-resonance R1rho relaxation outside of the fast exchange limit: an experimental study of a cavity mutant of T4 lysozyme, J. Biomol. NMR 26 (2003) 39–48.
[45] O. Trott, A.G. Palmer 3rd, R1rho relaxation outside of the fast-exchange limit, J. Magn. Reson. 154 (2002) 157–160.
[46] G. Lipari, A. Szabo, Model-free approach to the interpretation of nuclear magnetic resonance relaxation in macromolecules. 1. Theory and range of validity, J. Am. Chem. Soc. 104 (1982) 4546–4559.
[47] G. Lipari, A. Szabo, Model-free approach to the interpretation of nuclear magnetic resonance relaxation in macromolecules. 2. Analysis of experimental results, J. Am. Chem. Soc. 104 (1982) 4559–4570.
[48] G.M. Clore, A. Szabo, A. Bax, L.E. Kay, P.C. Driscoll, A.M. Gronenborn, Deviations from the simple two-parameter model-free approach to the interpretation of nitrogen-15 nuclear magnetic relaxation of proteins, J. Am. Chem. Soc. 112 (1990) 4989–4991.
[49] A.G. Palmer 3rd, M. Rance, P.E. Wright, Intramolecular motions of a zinc finger DNA-binding domain from Xfin characterized by proton-detected natural abundance 13C heteronuclear NMR spectroscopy, J. Am. Chem. Soc. 113 (1991) 4371–4380.
[50] M.P. Williamson, Using chemical shift perturbation to characterise ligand binding, Prog. Nucl. Magn. Reson. Spectrosc. 73 (2013) 1–16.